Supporting Online Material for

Alleviating Cancer Drug Toxicity by Inhibiting a Bacterial Enzyme

Bret D. Wallace, Hongwei Wang, Kimberly T. Lane, John E. Scott, Jillian Orans, Ja Seol Koo, Madhukumar Venkatesh, Christian Jobin, Li-An Yeh, Sridhar Mani, Matthew R. Redinbo*

*To whom correspondence should be addressed. E-mail: redinbo@unc.edu

Published 5 November 2010, *Science* **330**, 831 (2010)
DOI: 10.1126/science.1191175

This PDF file includes:

Supporting Online Material

Alleviating Cancer Drug Toxicity by Inhibiting a Bacterial Enzyme

Bret D. Wallace, Hongwei Wang, Kimberly T. Lane, John E. Scott, Jillian Orans, Ja Seol Koo, Madhukumar Venkatesh, Christian Jobin, Li-An Yeh, Sridhar Mani, and Matthew R. Redinbo

Experimental Methods

Expression and Purification of E. coli β-Glucuronidase. The full-length *E. coli* β-glucuronidase gene was obtained from bacterial genomic DNA and was cloned into the pET-28a expression plasmid (Novagen) with an N-terminal 6x-Histidine tag. BL21-DE3 competent cells were transformed with the expression plasmid and grown in the presence of kanamycin (25 μg/ml) in LB medium with vigorous shaking at 37 °C until an OD_{600} of 0.6 was attained. The expression was induced with the addition of 0.3 mM isopropyl-1-thio-D-galactopyranoside (IPTG) and further incubated at 37 °C for 4 hours. Cells were collected by centrifugation at 4500xg for 20 min at 4 °C in a Sorvall (model RC-3B) swinging bucket centrifuge. Cell pellets were resuspended in Buffer A (20 mM Potassium Phosphate, pH 7.4, 25 mM Imidazole, 500 mM NaCl), along with PMSF (2 μL/mL from 100 mM stock) and 0.05 μL/mL of protease inhibitors containing 1 mg/mL of aprotinin and leupeptin. Resuspended cells were sonicated and centrifuged at 14,500xg for 30 min in a Sorvall (model RC-5B) centrifuge to clarify the lysate. The cell lysate was flowed over a pre-formed Ni-NTA His-Trap gravity column and washed with Buffer A. The Ni-bound protein was eluted with Buffer B (20 mM Potassium Phosphate, pH 7.4, 500 mM Imidazole, 500 mM NaCl). Collected fractions were then tested for initial purity by SDS-PAGE. Relatively pure (~85%) fractions were combined and loaded into the Äktaxpress FPLC system (Amersham Biosciences) and passed over a HiLoad™ 16/60 Superdex™ 200 gel filtration column. The protein was eluted into 20 mM HEPES, pH 7.4, and 50 mM NaCl for crystallization and activity assays. Two milliliter fractions were collected based on highest ultraviolet absorbance at 280 nm. Fractions were analyzed by SDS-

PAGE (which indicated >95% purity), combined, and concentrated to 10 mg/mL for long-term storage at -80 °C.

Selenomethionine Substituted β-Glucuronidase. To express selenomethionine-substituted enzyme, B834 competent cells were transformed with pET-28a containing the β-glucuronidase gene. SelenoMet™ Medium and Nutrient Mix (AthenaES) was prepared for growth, with 50 mg of selenomethionine added for each liter of medium. The cells were grown at 37 °C until an OD_{600} of 0.6 was reached and then were induced with 0.3 mM IPTG. The temperature was lowered to 15 °C and the cultures were grown overnight with shaking. Purification was performed as for the wild-type enzyme (see above).

Crystallization, Data Collection, and Phasing. Crystals of *E. coli* β-glucuronidase were obtained at 2 mg/mL protein in 15% PEG3350, 0.2 M Magnesium Acetate, and 0.02% Sodium Azide at 16 °C. Crystals first appeared after 5 days, and grew to a final size of approximately 100x100x50 μm^3. Crystals were cryo-protected with perfluoropolyether vacuum pump oil (Sigma) and flash cooled in liquid nitrogen. Diffraction data were collected on the 22-BM beam line at SER-CAT (Advanced Photon Source, Argonne National Laboratory). Data was indexed and scaled using HKL2000 (*S1*) and X-GEN (*S2*). The crystals exhibited the space group C2, and the asymmetric unit contained two monomers. Selenomethionine data were collected to 2.9 Å and processed similarly. The PHENIX software suite (AutoSol) was utilized to locate heavy atom sites and to trace a portion of the model (*S3*). An initial model was built by hand in Coot using the SAD data and later used with Phaser for molecular replacement with a native data set and the inhibitor bound structures (*S4, S5*). The structure was refined using simulated annealing and torsion angle refinement with the maximum likelihood function target in CNS, and monitored using both the crystallographic R and cross-validating R-free statistics (*S6*). Ramachandran outliers were in loops with poor density relative to other regions of the model, and none exist within 20 Å of the enzyme's active site. Data collection and refinement statistics are presented in

Table S1. The software suite PHENIX was used for anisotropic B-factor and TLS refinement (*S3*). The model was manually adjusted using Coot and $2F_o$-F_c and F_o-F_c electron density maps (*S4*). The glucaro-δ-lactam model and definition files were generated using PRODRG (*S7*), and after a ligand search using Coot, was easily placed into electron density in the active site of both monomers.

Inhibitor Compounds. Purified protein was sent to NCCU-BRITE, the Biomanufacturing Research Institute and Technology Enterprise (BRITE) at North Carolina Central University (NCCU; Durham, NC), to screen various compound libraries for potential inhibitors. Four compounds were chosen for further analysis. The compounds (**Figure 1C**) were purchased from ASINEX, Inc. (the compound library development company ASINEX North America, in Winston-Salem, NC). Each compound was provided as a solid powder and dissolved in 100% dimethyl sulfoxide (DMSO) to various concentrations.

In Vitro β-Glucuronidase Assays. In vitro assays were conducted at 50 μL total volume in 96-well, clear bottom assay plates (Costar). Reactions consisted of the following: ten microliters Assay Buffer (5 μL of 5% DMSO, and 5 μL of 500 mM HEPES, pH 7.4), 30 μL substrate (various concentrations), 5 μL of an inhibitor solution (various concentrations), and 5 μL of 5 nM enzyme. Substrates used consisted of p-nitrophenyl glucuronide (PNPG) and phenolphthalein glucuronide (PheG) (Fig. 7SB) and were acquired from Sigma. The presence of the hydrolysis product of each, p-nitrophenol (PNP) and phenolphthalein (*S8*), was measured by absorbance at 410 nm or 540 nm, respectively. Reactions were allowed to proceed for 6 hours at 37 °C and were quenched with 100 μL of 0.2 M sodium carbonate. Absorbance was measured using a PHERAstar *Plus* microplate reader (BMG Labtech). Data acquired was analyzed using Microsoft Excel and Sigmaplot 11.0. Studies were conducted to show the conversion of SN-38G to SN-38 using purified *E. coli* β-glucuronidase. SN-38G was a generous gift from ENZON Pharmaceuticals, Bridgewater, NJ. The SN-38G enzymatic reactions were conducted in a PBS buffer, pH 7.4, with 10 μM SN-38G, and with and without purified β-glucuronidase at 0.5 μM. Enzyme and substrate were incubated

at 37 °C for 1 min and 1 hour. After the incubation period, the reaction mixture was acidified (HCl) and 10 μL of the reaction mixture was used to quantify SN-38/SN-38G concentrations. Concentrations were determined by a high-performance liquid chromatography (Phenomenex C 18- Jupiter [250 x 4.6, 5 μm]) assay with fluorescence detection using excitation and emission wavelengths of 368 and 515 nm, respectively. The zero enzyme control with SN-38G showed no conversion to SN-38. The mobile phase (20 mM ammonium acetate, pH 3.5, mobile phase A) and 100% acetonitrile containing 1% tetrahydrofuran (mobile phase B) was delivered at a flow rate of 0.5 mL/min. The mobile phase was filtered and degassed before use, and was freshly prepared for each run. The calibration curves (r^2=0.9998) were determined using a concentration range from 1 ng to 1 μg of SN-38G and SN-38. The LLQ was 1 ng/mL.

Mammalian Cell Survivability. The four compounds were tested for cytotoxicity in mammalian cells. CMT93 murine colon cancer cells, CaCO-2 human colon cancer cells, and HCT116 human colon cancer cells were grown and cultured in DMEM medium till confluent and adherent. Cells were counted and the appropriate dilutions were made to achieve a 50,000 cell count per reaction. Each cell line was aliquoted onto a 96-well assay plate and allowed to incubate at 37 °C in media for 16 hours prior to treatment with inhibitors. After incubation, 1 μL of each inhibitor, to achieve a final concentration of 100 μM, were added to the cells and further incubated for 24, 48, and 72 hours. Using the CellQuanti-Blue™ Cell Viability Assay Kit (BioAssay Systems), 10 μL of the CellQuanti-Blue™ Reagent was added to each reaction and incubated at 37 °C for 2 hours. After incubation with the reagent, fluorescence was measured with excitation at 544 nm and emission at 590 nm.

Mammalian β-Glucuronidase In Vitro Assays. Bovine liver β-glucuronidase was acquired in lyophilized form from Sigma. The protein was dissolved and the assay was conducted as previously published, using PNPG as the primary substrate for enzyme activity detection (*S9*). The reaction mixture contained 1 μM

bovine liver β-glucuronidase and 1 mM PNPG substrate. Each of the four inhibitors were tested for an effect on mammalian β-glucuronidase activity by adding a concentration range of 0 to 100 μM to the reaction mixture. The reaction was allowed to proceed for 6 hours and then quenched with 0.2 M Sodium Carbonate. Absorbance was measured at the appropriate wavelength, and the data analyzed using Microsoft Excel and SigmaPlot 11.0.

Cell-Based Inhibition Assays. HB101 *E. coli* cells, transformed with the pET-28a vector containing the β-glucuronidase gene, were grown to an OD_{600} of 0.6 in LB medium. The cells were then used in the *in vivo* assays to assess the glucuronidase activity and efficacy of the inhibitors. This assay was performed in a similar manner to the *in vitro* assay: ten microliters of substrate, 1 μL of inhibitor solution, and 40 μL of cells. Again, after 6 hours of incubation at 37 °C, the reaction was quenched with 100 μL of 0.2 M Sodium Carbonate. A β-glucuronidase gene (GUS) knockout cell-line (GMS407) was purchased from CGSC at Yale University. Absorbance was measured at the appropriate wavelength, either 410 nm or 540 nm. Cell survivability in the presence of the four inhibitors was assessed by plating a 10^{-5} dilution of 200 μL of saturated cells after incubation with 100 μM of each inhibitor for 6 hours. In addition, 1 mM of each hydrolysis product, 10 nM Tetracycline, and 2% DMSO (maximum concentration of DMSO when 100 μM inhibitor is added) were also tested for inhibitor effects on cell growth. Plated cells were allowed to incubate at 37 °C overnight, and colonies were counted to quantify the viability of the cells.

Anaerobic In Vivo Studies. For the anaerobic cell lines used, two types of growth medium and agar plates were prepared: MRS medium/agar was used for *Lactobacillus reuteri* and *Bifidobacterium infantis*, and BHI medium/agar for *Bacteroides vulgatus* and *Clostridium ramosum*. Anaerobic cell lines were graciously provided by the Sartor Lab at the University of North Carolina at Chapel Hill. MRS agar plates were prepared by combining MRS and agar powder, as well as 0.1 g L-cysteine. BHI plates were produced in a similar manner with the addition of 0.2 mL each of 5 mg/mL hemin and 0.1% resazurin.

Prior to streaking, plates were pre-equilibrated in an oxygen-free environment created in an anaerobic chamber and using the BD BBL™ GasPak™ Plus Anaerobic System Envelopes. One day before an assay was conducted, 5 mL overnight cultures, using the appropriate medium, were grown with no antibiotic present. Assay plates were prepared similar to the *E. coli* cell studies, and the reaction was allowed to progress in the anaerobic chamber for 6 hours. Absorbance data was collected after the reaction was quenched and analyzed.

Animal Studies. Irinotecan (CPT-11, Upjohn, Kalamazoo, MI) were purchased from LC Laboratories (#I-4122) as a hydrochloride salt (> 99% HPLC purified grade). For *in vivo* studies, the bacterial β-glucuronidase inhibitor was dissolved in 100% DMSO (2 mg/200 μL), then diluted with ddH_20 to a volume of 20 mL to reach a final concentration of 0.1 μg/μL. CPT-11 was dissolved in ddH_20 to make a stock of 20 mg/mL and stored at room temperature for a maximum of 2 hours prior to use. As vehicle control, all animals received an equivalent volume (compared to experimental groups) of 1% DMSO (ddH_20) solution. Healthy 6-8 week old female Balb/cJ mice (000651) were obtained from Jackson Laboratories, Bar Harbour, ME. The mice were housed in conventional metabolic cages (N=1/cage) and kept in a room under controlled temperature (20-22°C) and 12 hour day-night cycle. Animals had free access to water and conventional food without fortification. All studies were performed as approved by the Institutional Animal Ethics Committee (Albert Einstein College of Medicine, Bronx, NY). Mice were divided into four groups of 16 animals each: Group 1, vehicle controls receiving equivalent volume of ddH_2O intraperitoneally (ip) and 1% DMSO by oral gavage (~100 μL twice per day); Group 2, β-glucuronidase inhibitor 1 gavaged (10 μg/day) twice per day (every 10 hours) starting on day –1 with oral gavage of 1% DMSO, and ddH_2O ip once per day; Group 3, CPT-11 injected (50 mg/kg) ip once daily in the morning with oral gavage of 1% DMSO (~100 μL twice per day); Group 4, CPT-11 injected (50 mg/kg) ip once daily in the morning, and β-glucuronidase inhibitor 1 gavaged (10 μg/day) twice per day (every 10 hours). Total injected volume was identical for each animal. Previous studies indicate that

dosing at ~60-80 mg/kg/day for 4 days allows for observation of delayed diarrhea around 15 days, which is tolerable by germ-free and holoxenic mice (*S10*). A dosing scheme of 50 mg/kg/day, once daily for 9 days, was chosen with the intention of accelerating the onset of diarrhea while preventing death. As outlined previously, 50 mg/kg CPT-11 in mice is roughly equivalent to the 5 mg/kg typical human CPT-11 dose based on differences in body surface area (BSA) (*S10, S11*). Body weight, stool consistency and occult blood in stool were monitored daily using methods previously published (*S12*). On day 9, anal openings were digitally photographed to demonstrate the nature of diarrhea. GI symptoms in Group 3 started as early as day 2 and up to day 7, and included decreased appetite and bowel movements, and reduced body movement and body weight. Some animals in Group 3 required euthanization by day 9 or 10; all other animals in Group 3 and the other groups were euthanized on day 11. Mice were examined daily for signs of diarrhea (fecal staining of skin, lose watery stool) and bloody diarrhea (black sticky stool). After sacrifice, large intestines were formalin-fixed and paraffin embedded for routine H&E histopathologic examination to arrive at a histologic score as follows (*S13*). For cell infiltration of inflammatory cells, rare inflammatory cells in the lamina propria were counted as 0; increased numbers of inflammatory cells, including neutrophils in the lamina propria as 1; confluence of inflammatory cells, extending into the submucosa as 2; and a score of 3 was given for transmural extension of the inflammatory cell infiltrate. For epithelial damage, absence of mucosal damage was counted as 0, discrete focal lymphoepithelial lesions were counted as 1, mucosal erosion/ulceration was counted as 2, and a score of 3 was given for extensive mucosal damage and extension through deeper structures of the bowel wall. The two subscores were added and the combined histologic score ranged from 0 (no changes) to 6 (extensive cell infiltration and tissue damage). Statistical analysis of the animal data were reported as mean ($\pm$ SD) unless otherwise noted. Statistical analysis was performed using GraphPad prism software version 4.0 (San Diego, CA). Student's unpaired *t*-test was used to test the significance of differences in diarrhea and related events between controls and inhibitor treated groups.

Supporting Information and Data

CPT-11 and SN-38. The average incidence of sever diarrhea in patients treated with CPT-11 is ~30-40%, of which 10% required hospitalization (*S14-S18*). Updated formulations of CPT-11 and newer camptothecin analogs have not solved the toxicity problems associated either with glucuronidation or other side effects (*S19, S20*). It is not clear that reabsorption of SN-38 from the GI plays a significant role in anti-tumor efficacy. Recirculation of SN-38 from intestinal reabsorption would be expected to result in second or multiple peaks in blood over time, which are not observed (*S21-S25*). Local absorption directly to colon tumors may occur, but, to date, intestinal SN-38 concentrations have been associated with toxicity not efficacy (*S26*).

SN-38G Conversion by β-Glucuronidase. Purified *E. coli* β-glucuronidase was incubated with SN-38G substrate and production of SN-38 was monitored by HPLC as indicated in Fig. S1. No conversion to SN-38 was observed without enzyme added.

E. coli β-Glucuronidase Crystal Structure. The 2.4 Å resolution GDL-bound structure reveals a single clear binding mode of the inhibitor within the *E. coli* β-glucuronidase active site (Figs. S3A, S3B). GDL forms direct contacts with the catalytic residues E413 and E504, and with five other amino acids at the active site (D163, R562, K568, Y472, H330) (Fig. S3C). While the inhibitor-bound structure shares 1.2 Å overall r.m.s.d. with the apo enzyme, significant shifts in backbone position ($\geq$ 2.8 Å) occur adjacent to the catalytic site (Fig. S3B). The entrance to the active site in the apo structure is occluded by the 466-476 loop that contains tyrosines 468, 469 and 472; this loop would clash sterically with the observed position of the GDL inhibitor. In the inhibitor-bound structure, however, this loop shifts to relocate these aromatic residues 7-14 Å away and allow GDL binding (Fig. S3B). The opening of the active site increases in area from 10.9 $Å^2$ to 20.8 $Å^2$ upon inhibitor binding, and allows Y472 to form a direct contact

with the GDL molecule (Fig. S3B). Thus, a conformational change is critical to ligand binding to the *E. coli* β-glucuronidase active site.

Inhibitor Discovery via High-Throughput Screening. The conversion of p-nitrophenyl glucuronide (PNPG) to p-nitrophenol (PNP) (*S27*), which absorbs at 410 nm, was used, as well as an assay involving the conversion of phenolphthalein glucuronide (PheG) to phenolphthalein (*S8*, *S27*), which absorbs at 540 nm (Fig. S7B). Both assays (PNPG and PheG) were validated *in vitro* and in living cells, and the wavelengths monitored did not overlap with absorbance characteristics of putative inhibitors. For cell-based assays, control experiments established that the activity detected was dependent on β-glucuronidase. *E. coli* cells lacking a β-glucuronidase gene showed no enzyme activity using PNPG as a substrate; however, when the *E. coli* β-glucuronidase was expressed, enzyme activity increased accordingly (Fig. S15). In addition, the *E. coli* cells lacking a β-glucuronidase gene showed no phenotypic abnormalities. High-throughput screening was conducted at the Biomanufacturing Research Institute and Technology Enterprise (BRITE) Center of Excellence at North Carolina Central University. BRITE has a total chemical collection of 410,000 compounds. In this case, a diversity set of 10,240 compounds with molecular weights around 500 Da from ASINEX, was screened. The four compounds were chosen because they were based on a similar chemical scaffold but showed a range of *in vitro* and cell-based efficacies from ~15 nM to 1 μM. A method of use patent has been filed for the application of these compounds to CPT-11-induced toxicity. The use of these compounds for other clinical applications has not been reported to our knowledge.

Fig. S1

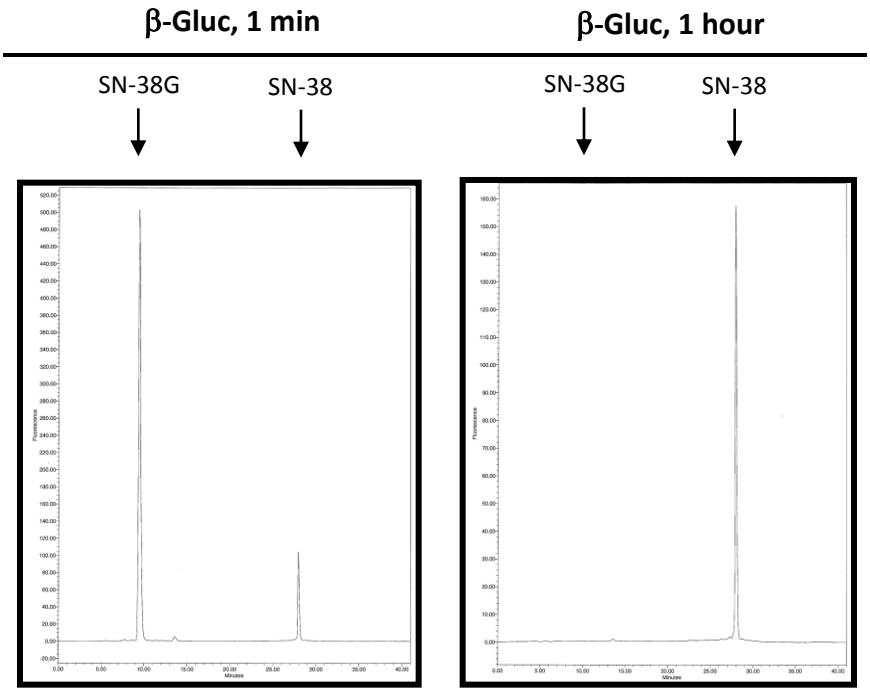

	SN-38G Area (% Area)	**SN-38** Area (% Area)
β-Glucuronidase, 1 min	8919774 (88.49)	1165180 (11.51)
β-Glucuronidase, 1 hour	0(0)	1885840 (100)

Fig. S1. *Top:* Incubations of SN-38G with β-glucuronidase for 1 min. (left) and 1 hour (right). Retention times for SN-38G and SN-38 were 9.4 min. and 27.9 min., respectively. *Bottom:* Peak analysis in which "% Area" is peak area remaining as a percent of the total area constituting the SN-38G + SN-38 peaks. The experiment was performed once in duplicate.

Fig. S2

Protein	PDB ID	Z-Score	RMSD	# Residues Aligned	# Residues Total	% Identity
Homo sapiens Beta-Glucuronidase	3HN3	48.0	1.2	571	608	45
Escherichia coli Beta-Galactosidase	3DYP	33.1	2.4	511	1011	22
Arthrobacter sp. C2-2 Beta-Galactosidase	1YQ2	31.7	2.7	509	1020	23
Cellvibrio mixtus Mannosyl-Oligosaccharide Glucosidase	1UUQ	27.4	2.4	282	410	15
Bacteroides thetaiotamicron Beta-Mannosidase	2VQU	24.5	3.1	497	839	15

Fig. S2. Sample of similar structures identified by DALI (*S28*). The native β-glucuronidase structure (3K46) was employed, and a subset of the 886 structures* is presented. The root mean square deviation (RMSD) in Å is for superimposed Cα positions. *Z-scores between 48.0 to 10.

Fig. S3

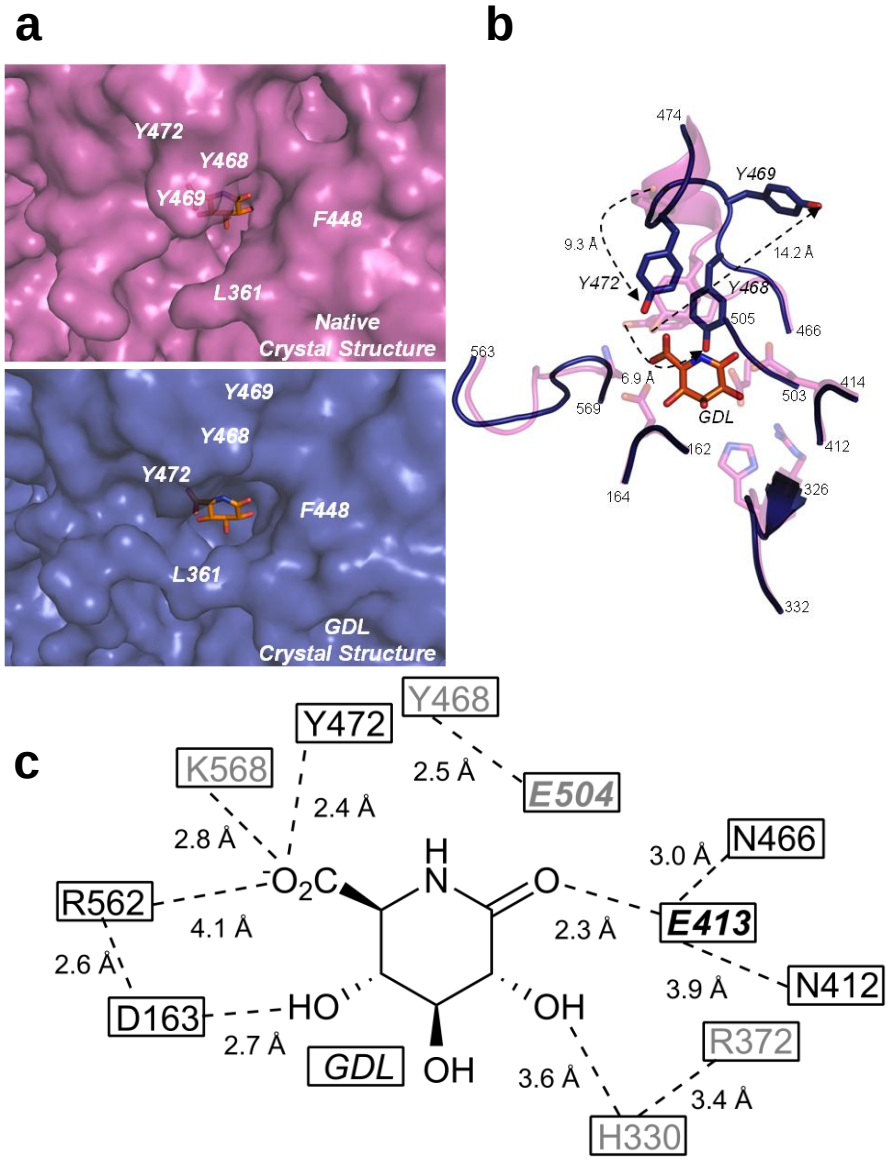

Fig. S3. A) Surface model of the active sites of the native and GDL-bound crystal structures. The GDL molecule is overlaid in the native structure (top, magenta) to show the major steric clashes with the residues labeled that encompass the active site. In the inhibitor bound structure (bottom, blue), the active site is opened, with movement of the surrounding tyrosines to allow for easy fitting of the compound in the active site. **B)** A cartoon and stick overlay of the native and GDL-bound active sites. As previously stated, the native (magenta) has a closed active site due to Y468, Y469, Y472. With the GDL-bound structure (blue), Y468 and Y472 flip-in to the active site to form key interactions with the compound and with E504, the nucleophilic residue. Tyrosine 469 flips away from the active making room for the carboxylic functional group of the inhibitor. **C)** Diagram of the β-glucuronidase active site with the GDL molecule bound. Key residues (and distances) are labeled that interact with either the compound or the catalytic residues facilitating the enzymatic reaction. Residues in gray are beneath and those in black are equal or above the plane of the GDL molecule in the crystal structure. The two residues in italics, E413 and E504, are the catalytic residues.

Fig. S4

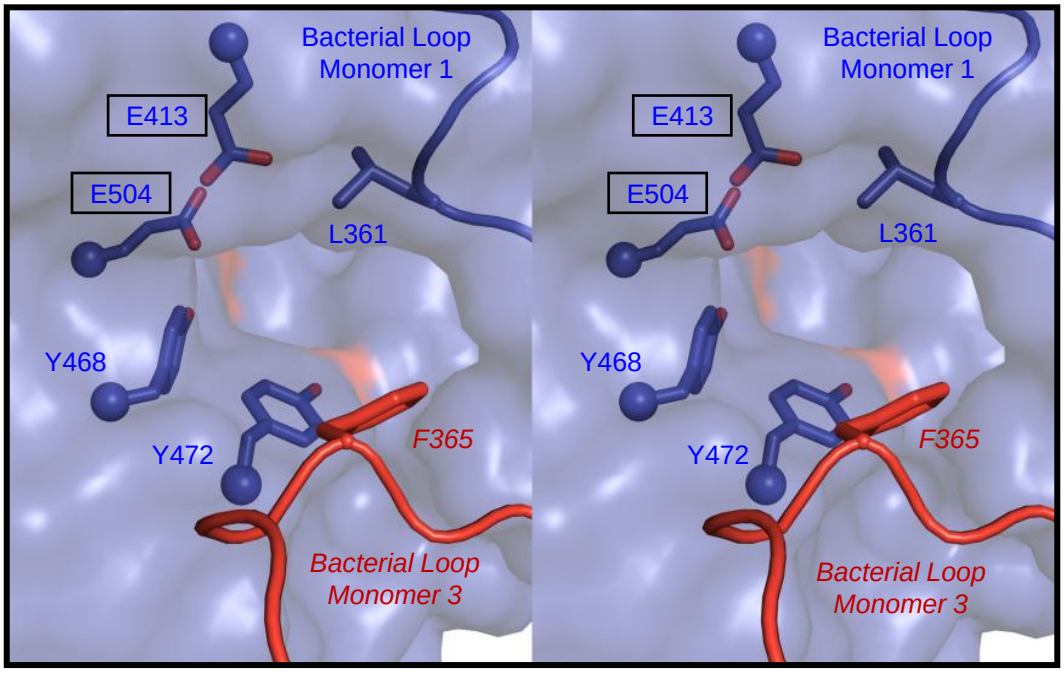

Fig. S4. Stereoview of the active site of *E. coli* β-glucuronidase highlighting the catalytic E413 and E504 residues, as well as the positions of loops unique to the bacterial β-glucuronidase. The active site of each monomer contains a loop from that monomer (blue), as well as a neighboring monomer in the catalytic tetramer.

Fig. S5

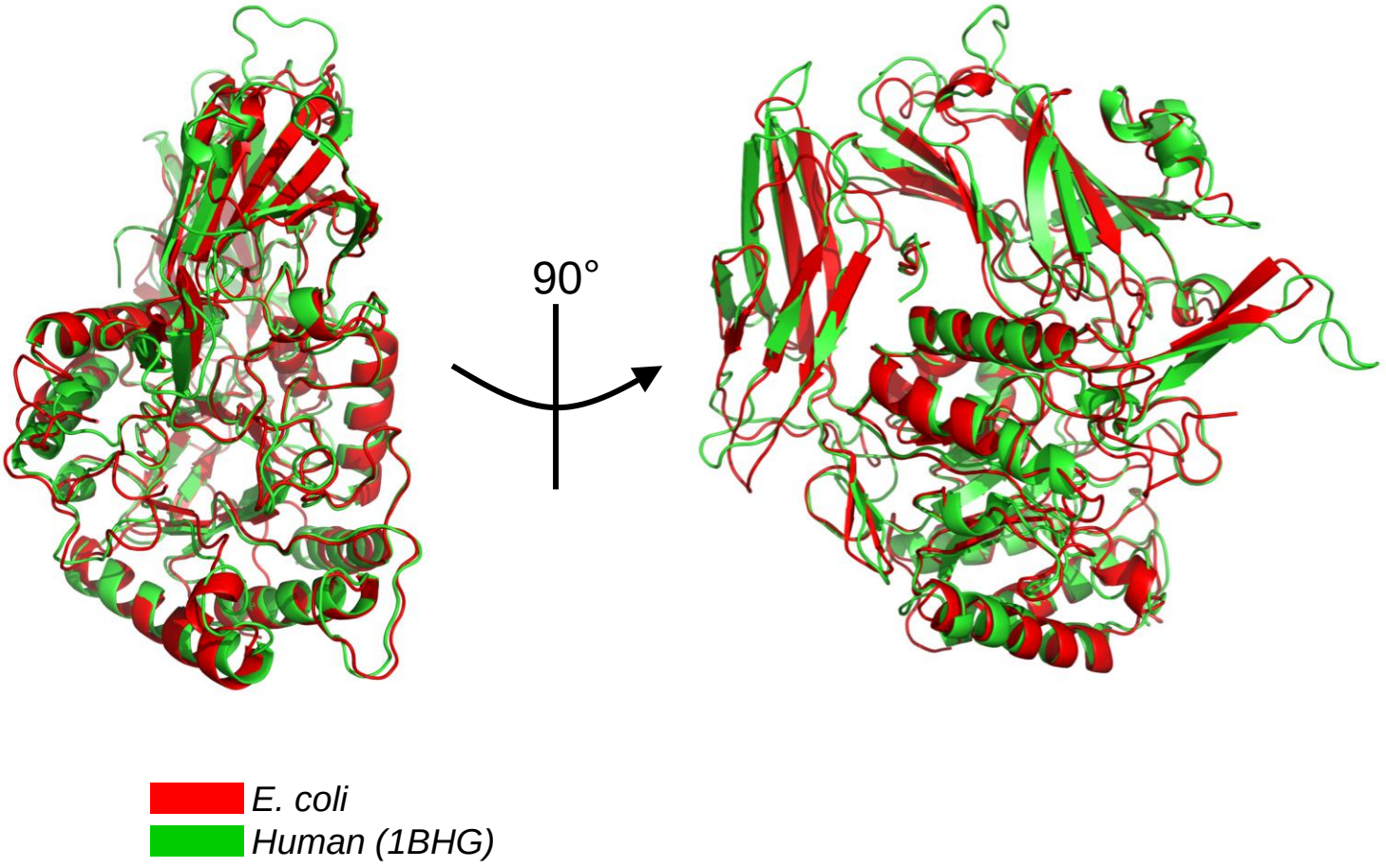

Fig. S5. Native monomer overlay of Human (red, 1BHG) and *E. coli* (green) β-glucuronidase.

Fig. S6

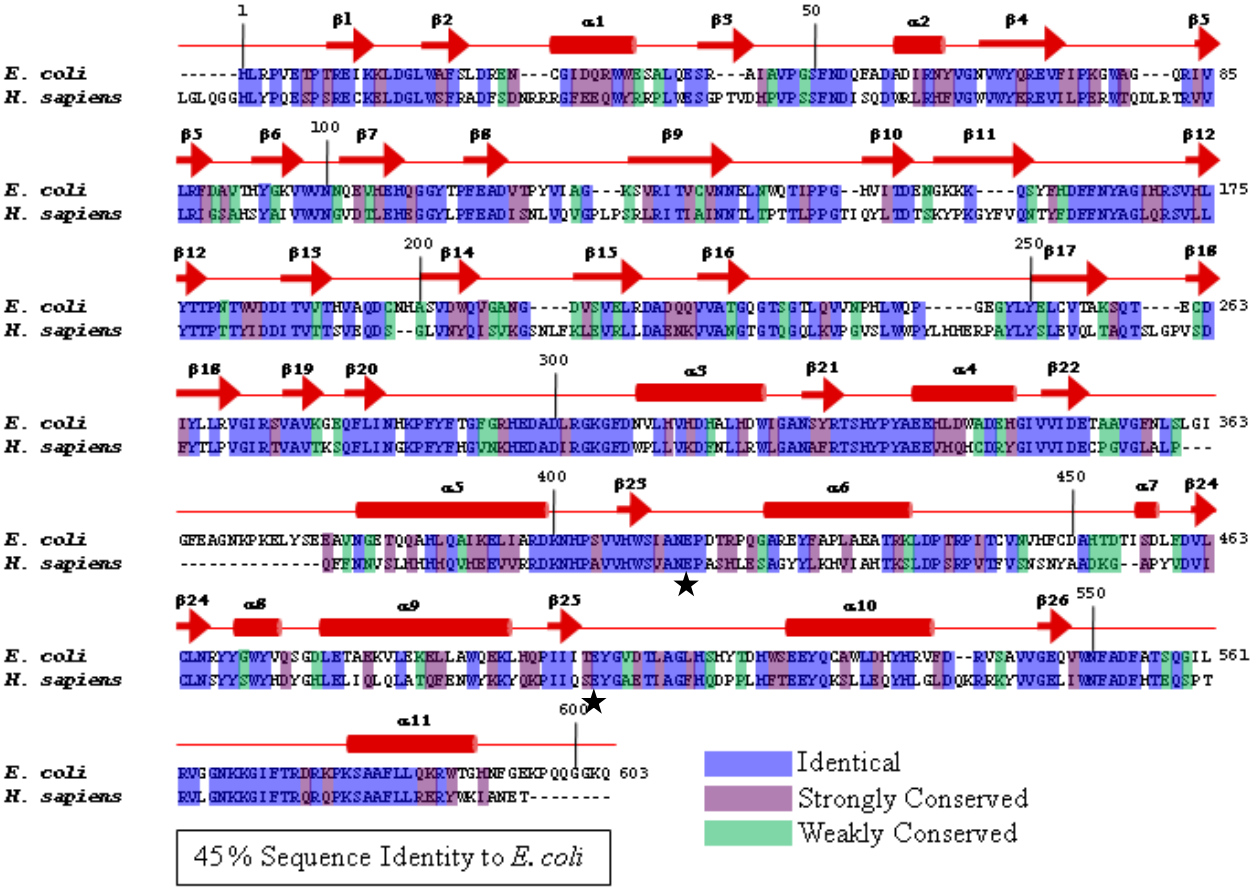

Fig. S6. Sequence alignment of β-glucuronidase from *H. sapiens* against *E. coli* sequence. Human β-glucuronidase has a 45% sequence identity to the *E. coli* enzyme. Secondary structure of the *E. coli* crystal structure are displayed above the sequence, and the indicated numbers are relative to the *E. coli* sequence. The two starred (★) residues indicate the conserved catalytic residues, E413 and E504.

Fig. S7

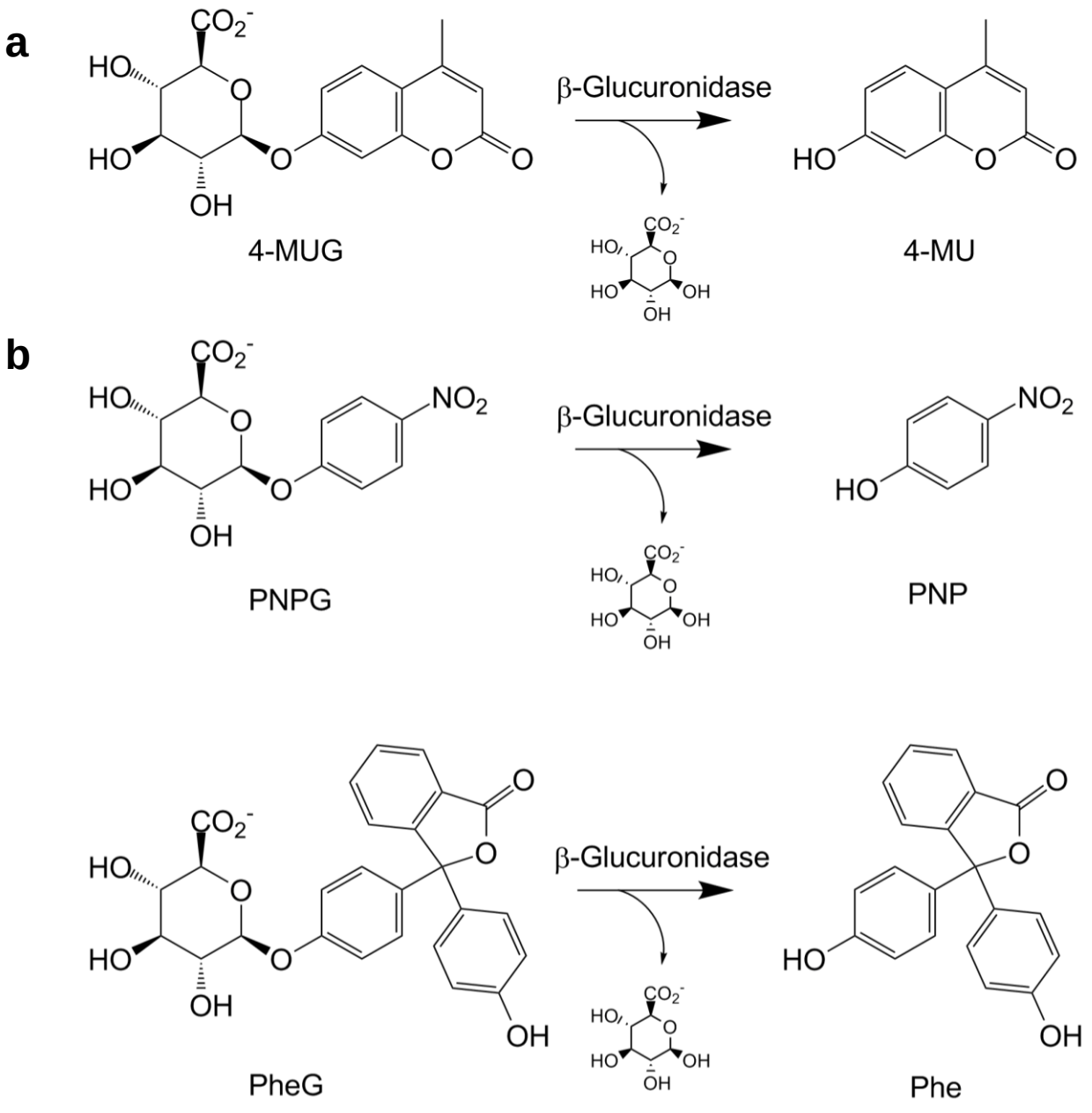

Fig. S7. Hydrolysis reactions catalyzed by β-glucuronidase in the three activity assays utilized. The hydrolysis products of each produced the necessary signal to detect β-glucuronidase activity. **A)** Activity assay scheme detailing the conversion of 4-methylumbelliferyl-glucuronide (4-MUG) to the fluorescent 4-methylumbelliferone (4-MU). **B)** Secondary activity assay schemes detailing the conversion of p-nitrophenyl glucuronide (PNPG) and phenolphthalein glucuronide (PheG) to their respective absorbent products, p-nitrophenol (PNP) and phenolphthalein (Phe).

Fig. S8

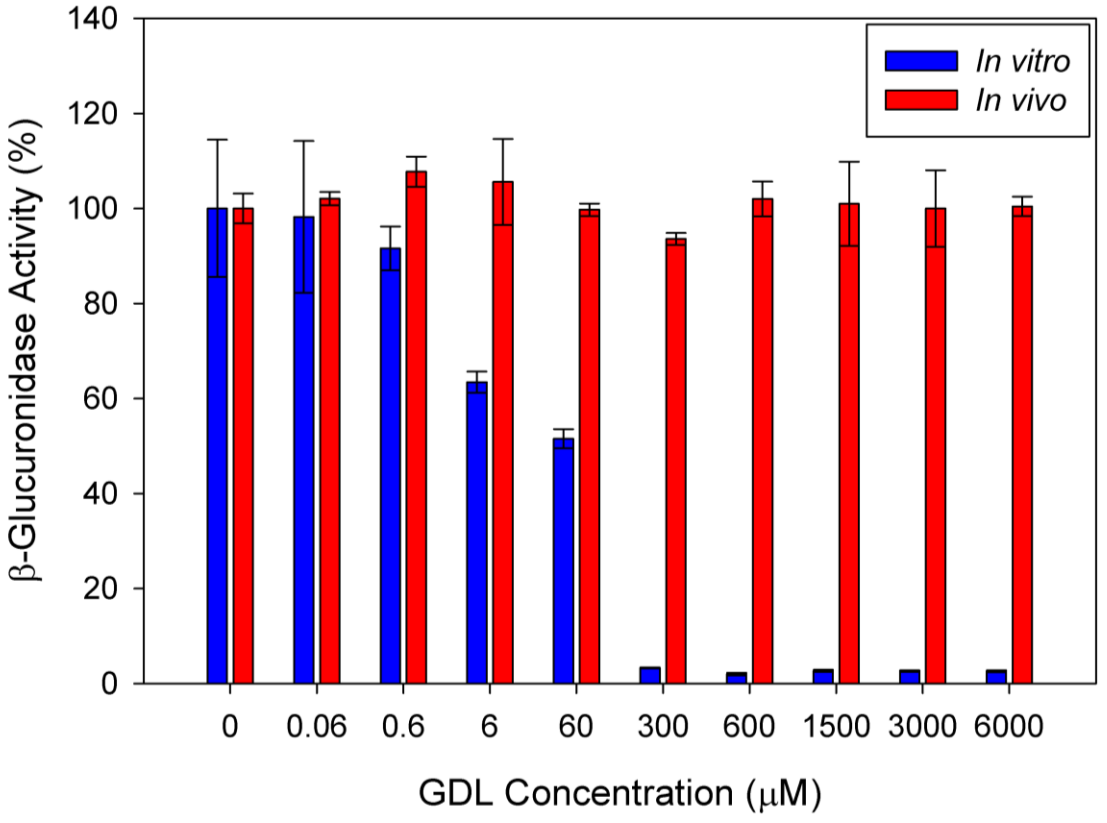

Fig. S8. Graph showing the reduction in β-glucuronidase activity using the known glucaro-δ-lactam inhibitor and 1 mM PNPG. IC50 values were calculated and GDL had a weak IC50 of 45 ± 3.1 μM (SD, N=3) *in vitro*; however, GDL was ineffective (no IC50 could be calculated) *in vivo*.

Fig. S9

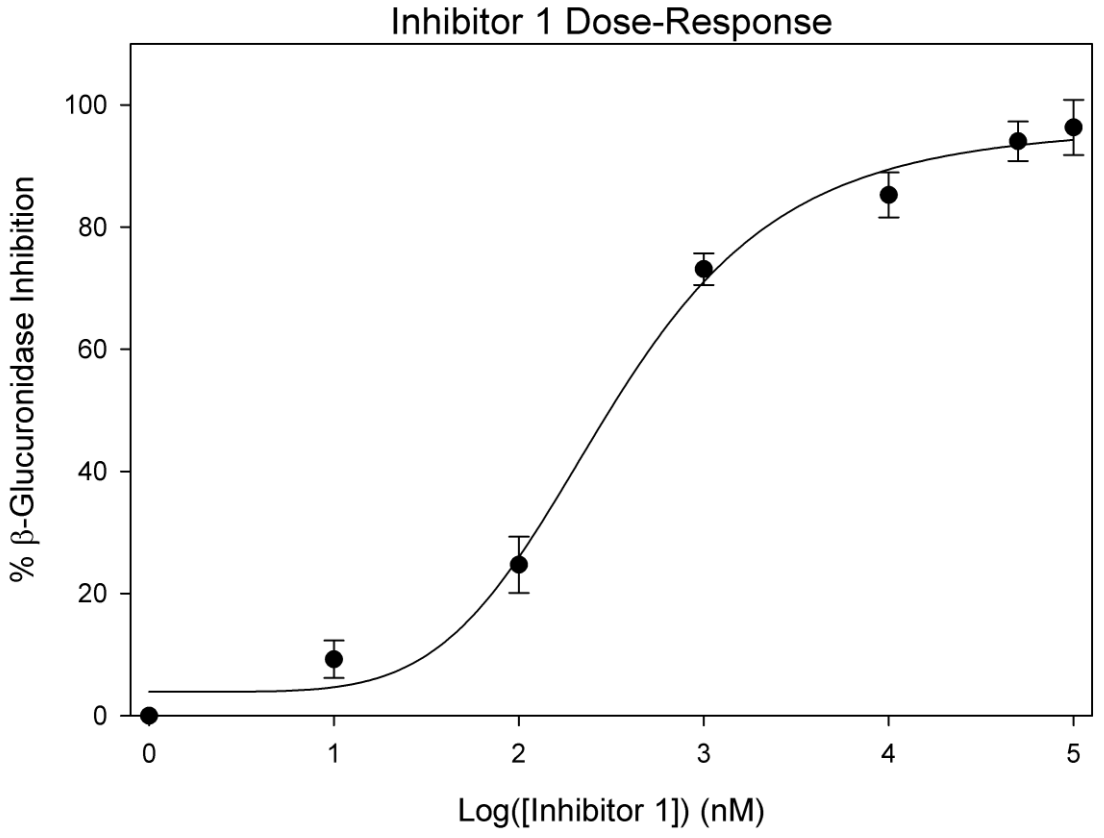

Fig. S9. Dose-response curve showing the increase in inhibition with increasing concentrations of Inhibitor 1. At concentrations above 1 μM there is greater than 80% inhibition of the enzyme. The IC50 is calculated to be 283 ± 26.1 nM (SD, N=3).

Fig. S10

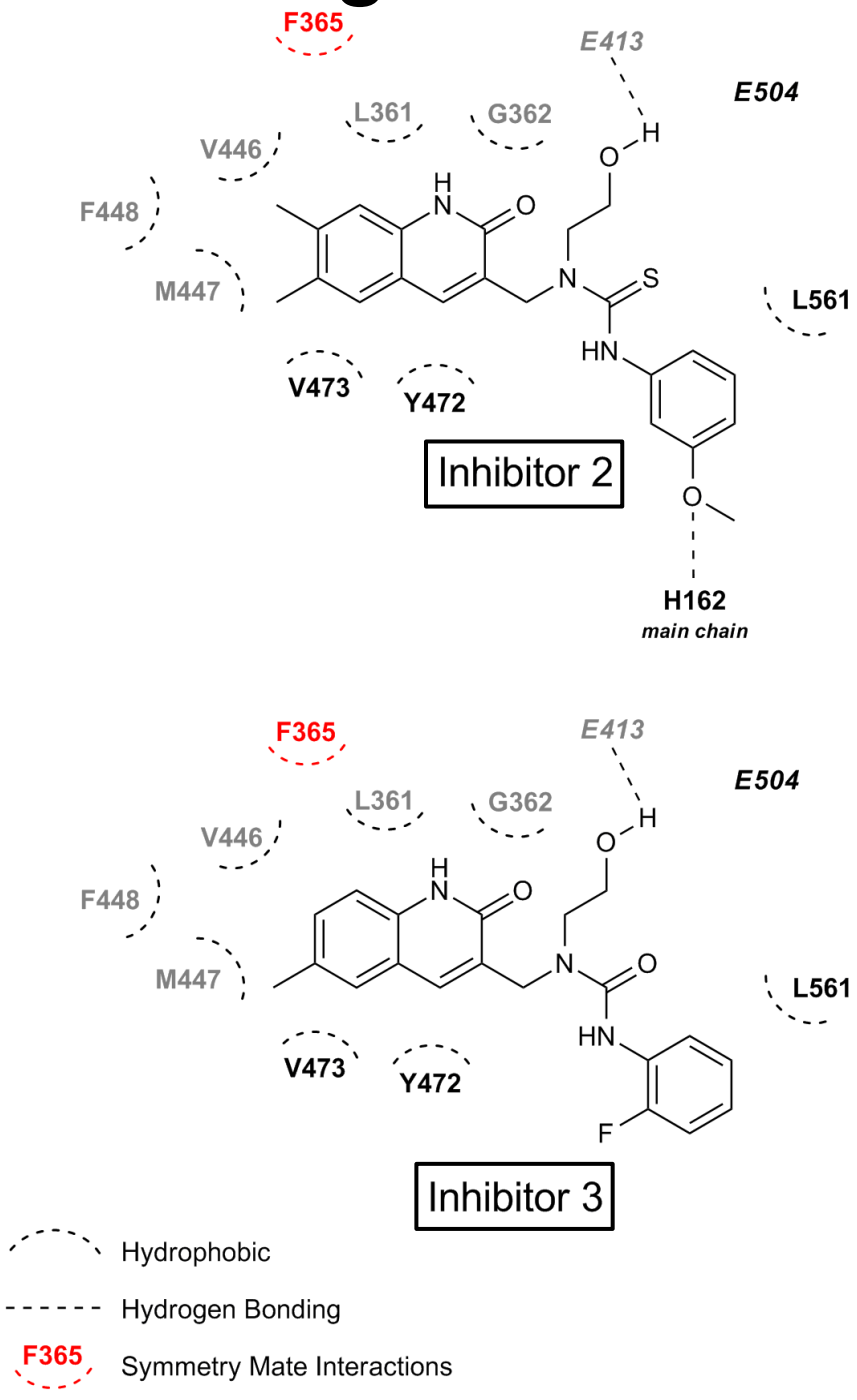

Fig. S10. Key interactions formed between residues and bound inhibitors found in the crystal structures. Almost all interactions are conserved between the two inhibitors, with the exception of a hydrogen bond formed between the inhibitor and H162. As can be seen, the majority of the interactions are hydrophobic, formed between residues surrounding the active site as well as key interactions with the bacterial loop (L361 and F365 from the symmetry mate).

Fig. S11

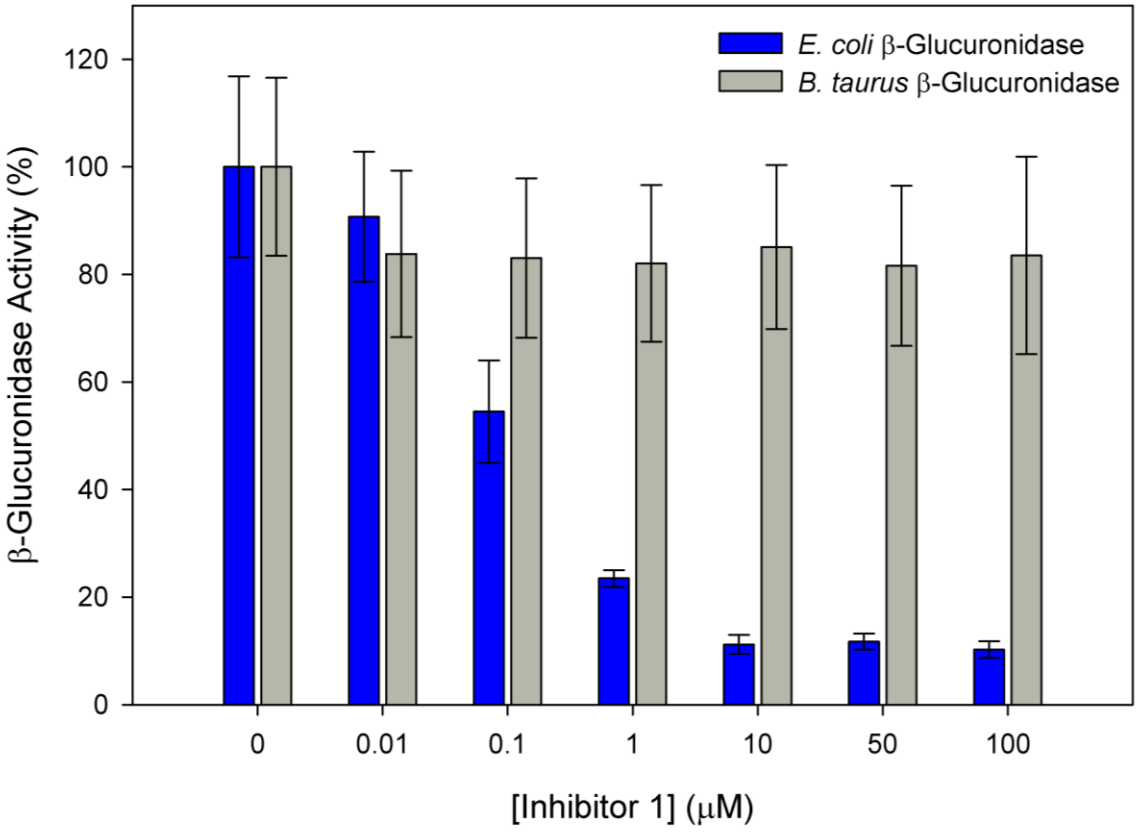

Fig. S11. Inhibitor 1 impacts *E. coli* β-glucuronidase activity *in vitro*, but not that of bovine liver β-glucuronidase. Error bars represent standard deviation, where N=3.

Fig. S12

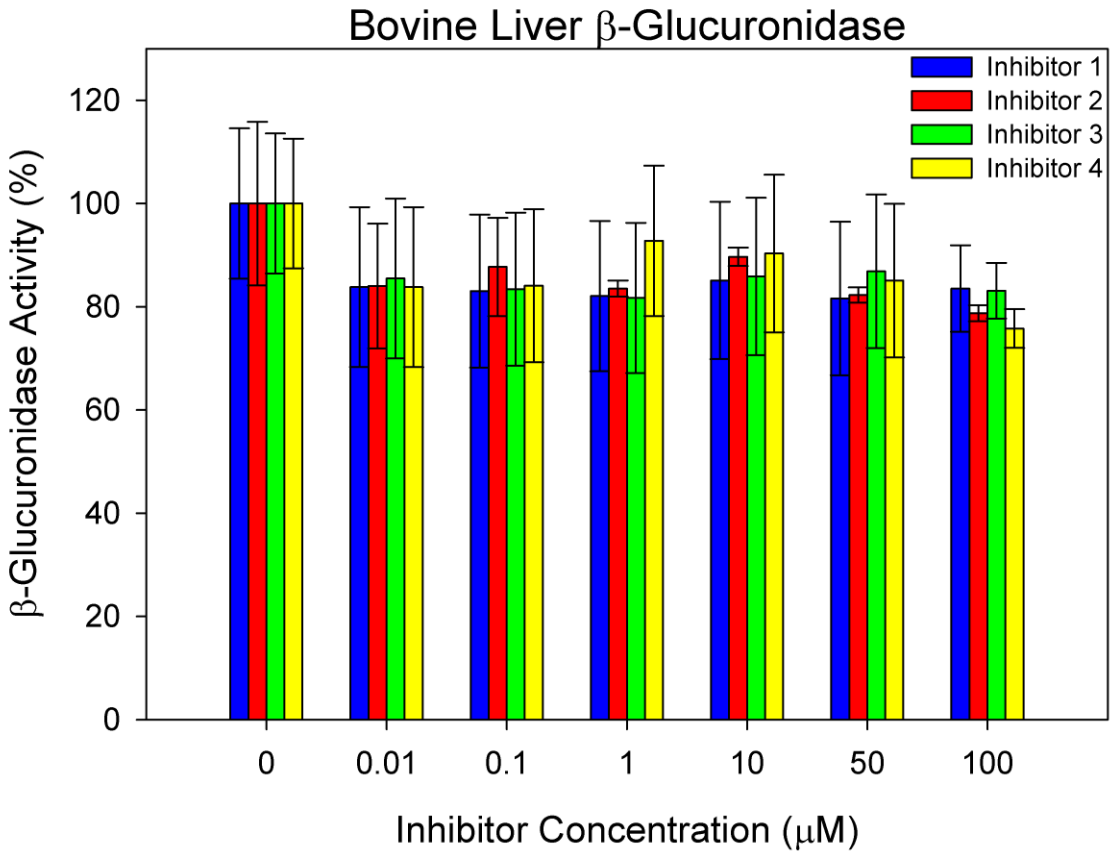

Fig. S12. Results of the bovine liver β-glucuronidase activity assay in the presence of Inhibitors 1-4. In all four cases, there is little to no reduction in bovine liver β-glucuronidase activity with increasing inhibitor concentration. As such, these inhibitors are ineffective against the mammalian bovine liver β-glucuronidase. Error bars represent standard deviation, where N=3.

Fig. S13

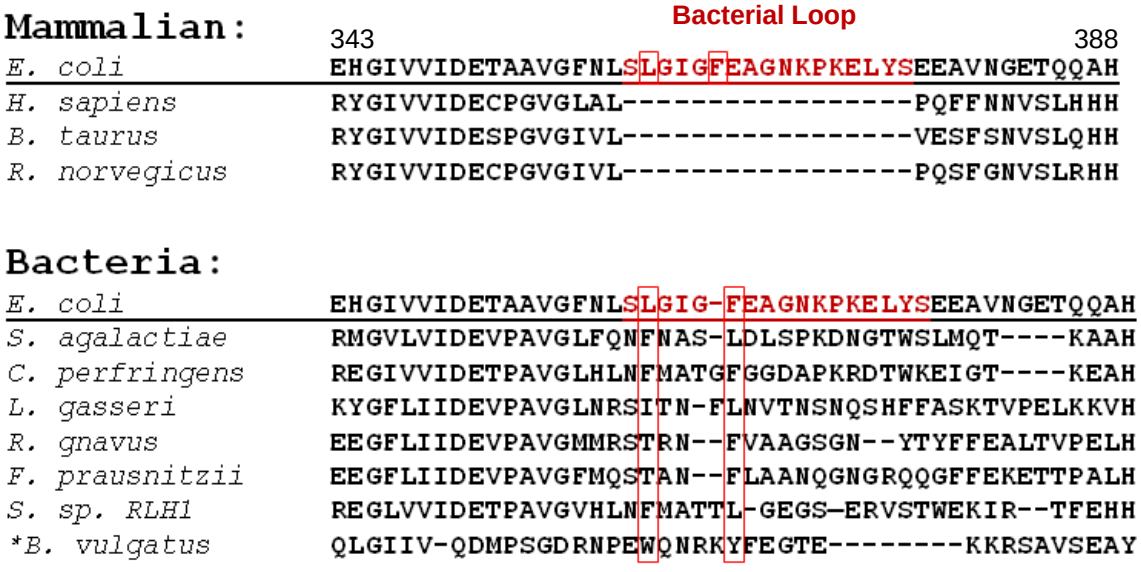

Fig. S13. The 360-376 loop in *E. coli* β-glucuronidase is present in bacterial enzymes but missing from the mammalian orthologues. According to the inhibitor-bound crystal structures, residues such as the L361 and F365 (boxed in red), make hydrophobic and side chain interactions with the inhibitors. F365 makes a critical contact with the inhibitor in a different monomeric subunit (see **Figure 2B**). G362 and G364 in *E. coli* β-glucuronidase are in non-glycine-only regions of Ramachandran space; thus, these glycines are not critical to bacterial loop positioning. *Note that no explicit β-glucuronidase sequence has been identified, though *Bacteroides vulgatus* is known to have β-glucuronidase activity; however, a conserved family 2 glycosyl hydrolase is found. Part of the loop is absent from *B. vulgatus*; however, a consecutive tyrosine and phenylalanine to possibly replace the F365 from *E. coli*, as well as a tryptophan in place of L361, which could easily form ring stacking interactions with the inhibitors. Sequence alignments were generated by ClustalW (*S29*) using the complete β-glucuronidase or putative β-glucuronidase primary structures and were not further manipulated.

Fig. S14

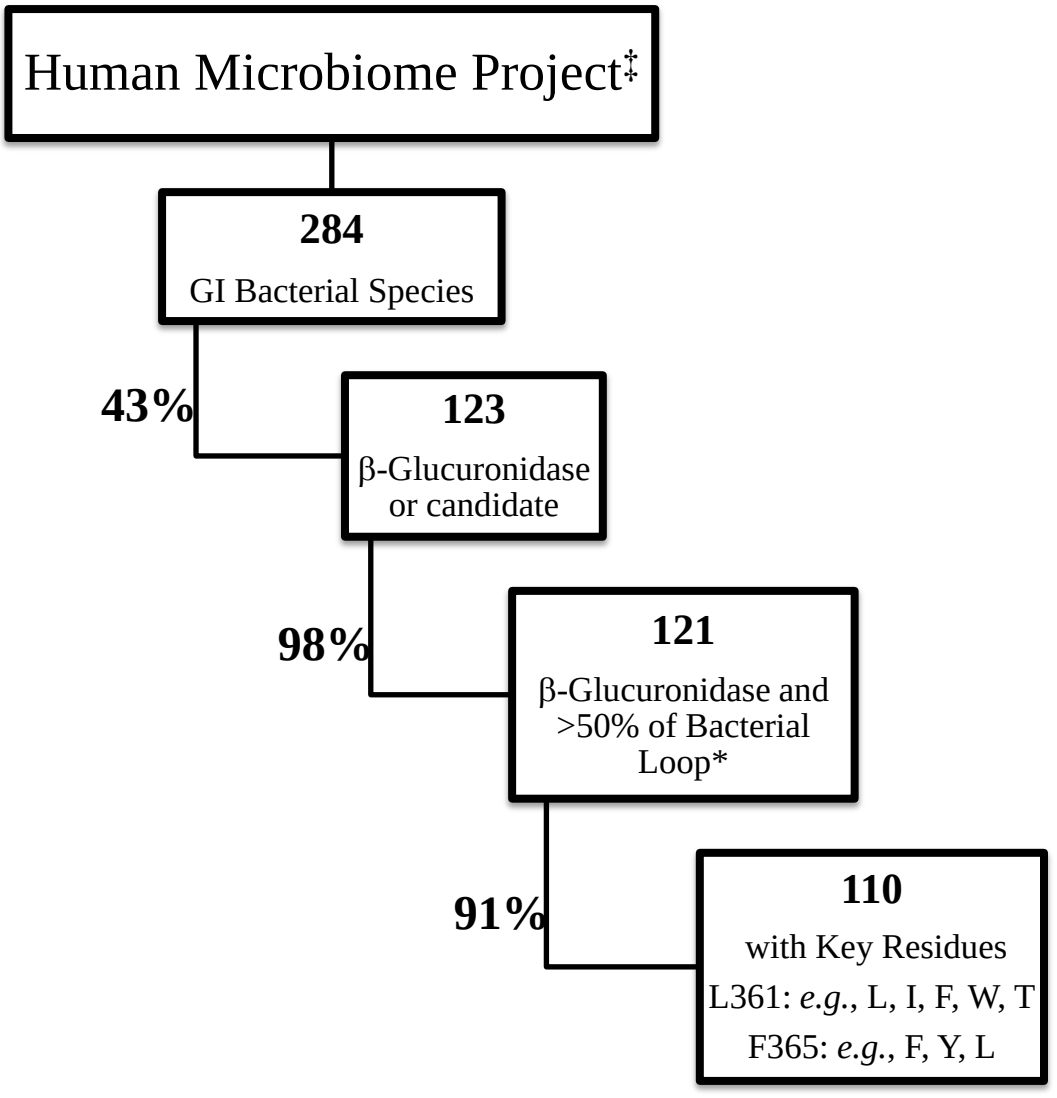

Fig. S14. The Human Microbiome Project (*S30*) database was searched to assess the conservation of the bacterial loop in a variety of gastrointestinal (GI) bacterial β-glucuronidases. Of the 284 species known to be in the GI tract that have been sequenced, 43% contained the β-glucuronidase gene or a possible candidate. Ninety-eight percent of these β-glucuronidase containing species maintained at least 50% of the bacterial loop; 91% of these bacterial loops retained good conservation of the residues shown to be critical for inhibitor binding in the *E. coli* enzyme. ‡ Search conducted June 29, 2010. * Gene products that contain at least the N-terminal half of the bacterial loop.

Fig. S15

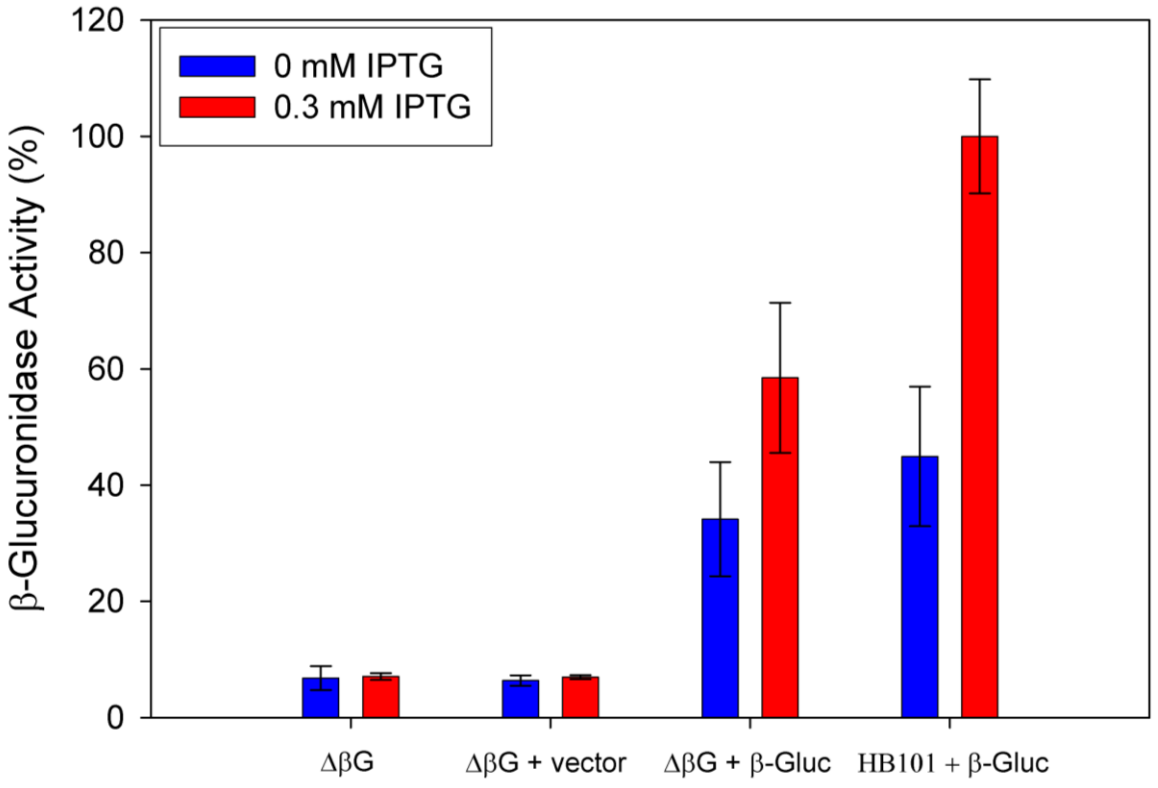

Fig. S15. Results of the knockout and IPTG control experiments. An *E. coli* cell line with the β-glucuronidase gene knocked out (see Materials and Methods) showed no activity in the activity assays with and without IPTG induction. This same cell line transformed with the pET-28a vector also exhibited no β-glucuronidase activity. Finally, the knockout and HB101 cell lines (used in all the *E. coli in vivo* experiments) transformed with the pET-28a vector containing the gene both showed activity with and without (possibly leaky expression) IPTG induction. Error bars represent standard deviation, where N=3.

Fig. S16

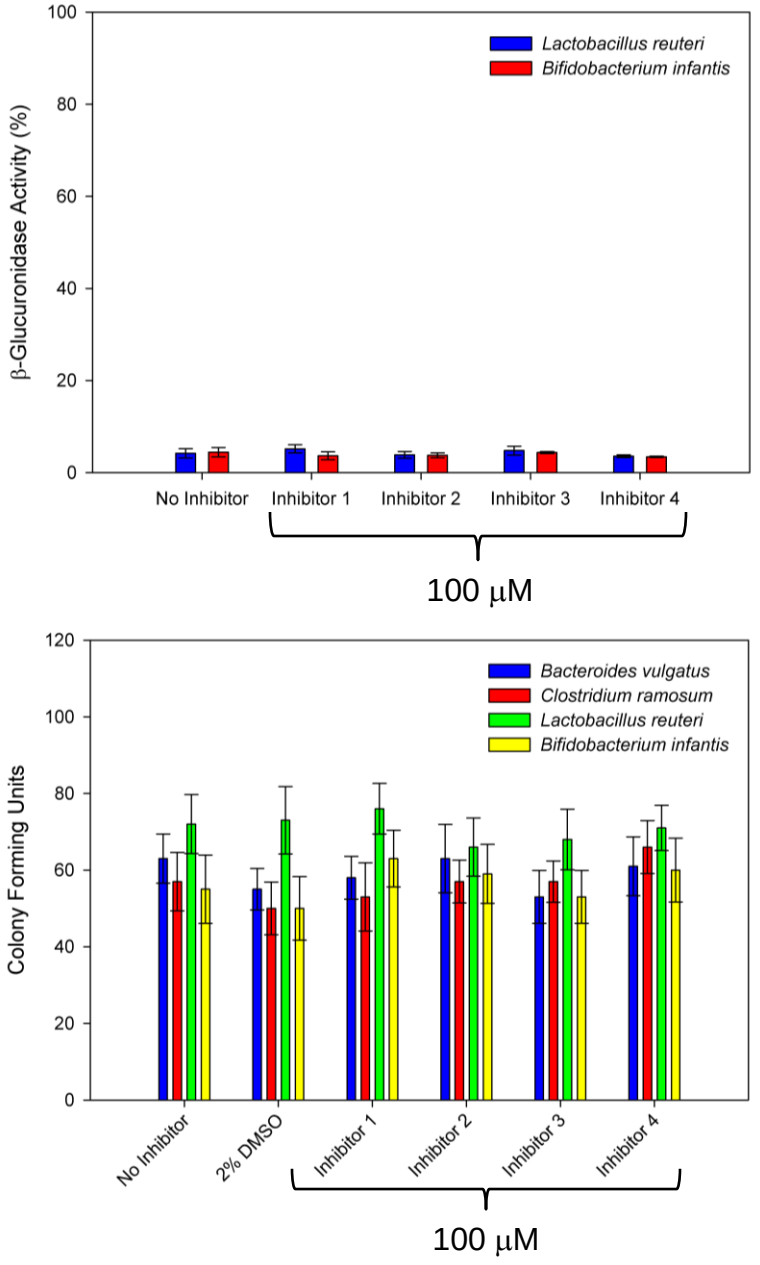

Fig. S16. Anaerobic cell-based activity assay for *Lactobacillus reuteri* and *Bifidobacterium infantis*. Neither species contain the β-glucuronidase gene, and as expected, show no β-glucuronidase activity in the anaerobic cell-based assays conducted. All four anaerobic species were incubated with 100 μM Inhibitor and plated to assess the viability of each cell line in the presence of inhibitor. In the case of each inhibitor cell growth was not effected. Error bars represent standard deviation, where N=3.

Fig. S17

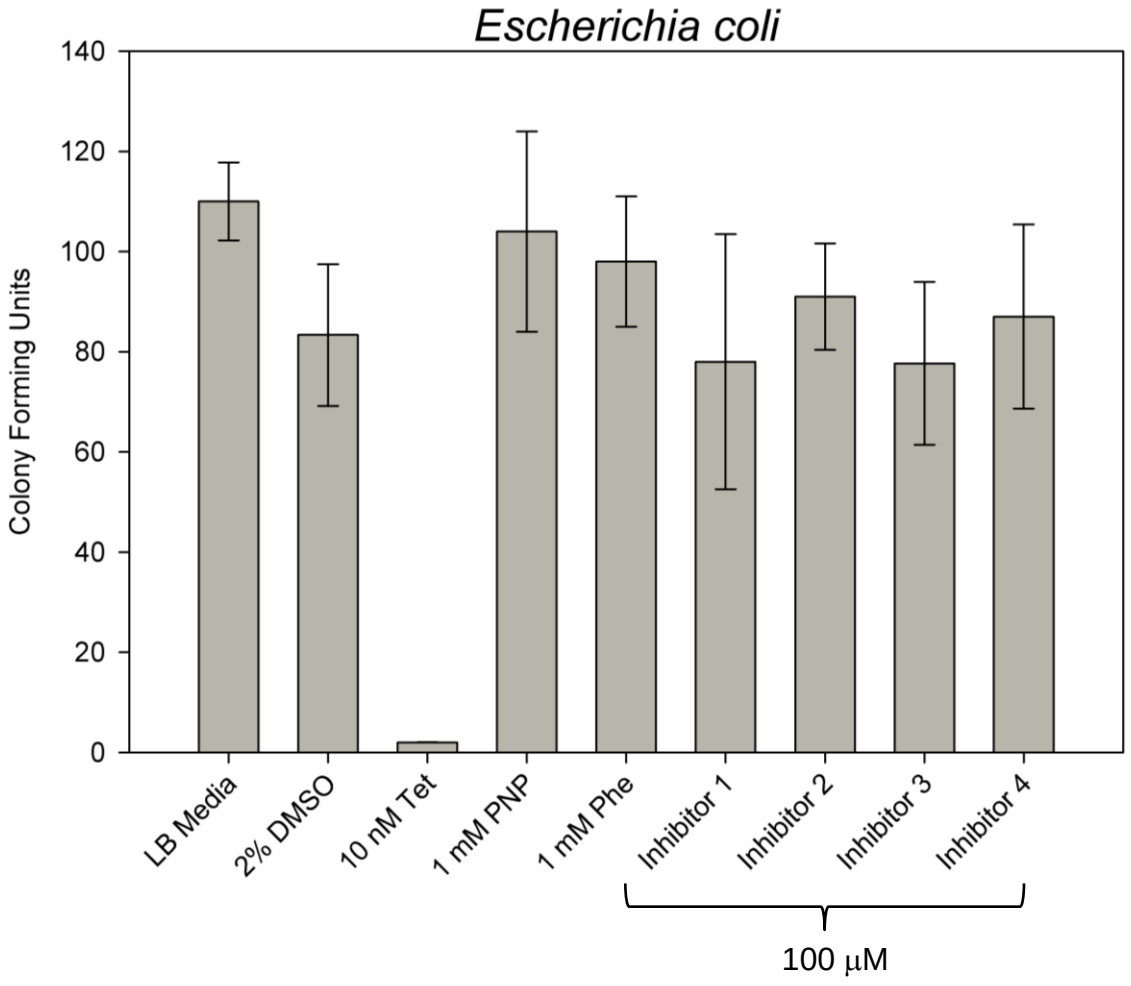

Fig. S17. Inhibitors 1-4, as well as the assay products 1 mM (PNP) and 1 mM (Phe), do not impact bacterial cell survival, unlike tetracycline (Tet). Error bars represent standard deviation, where N=3.

Fig. S18

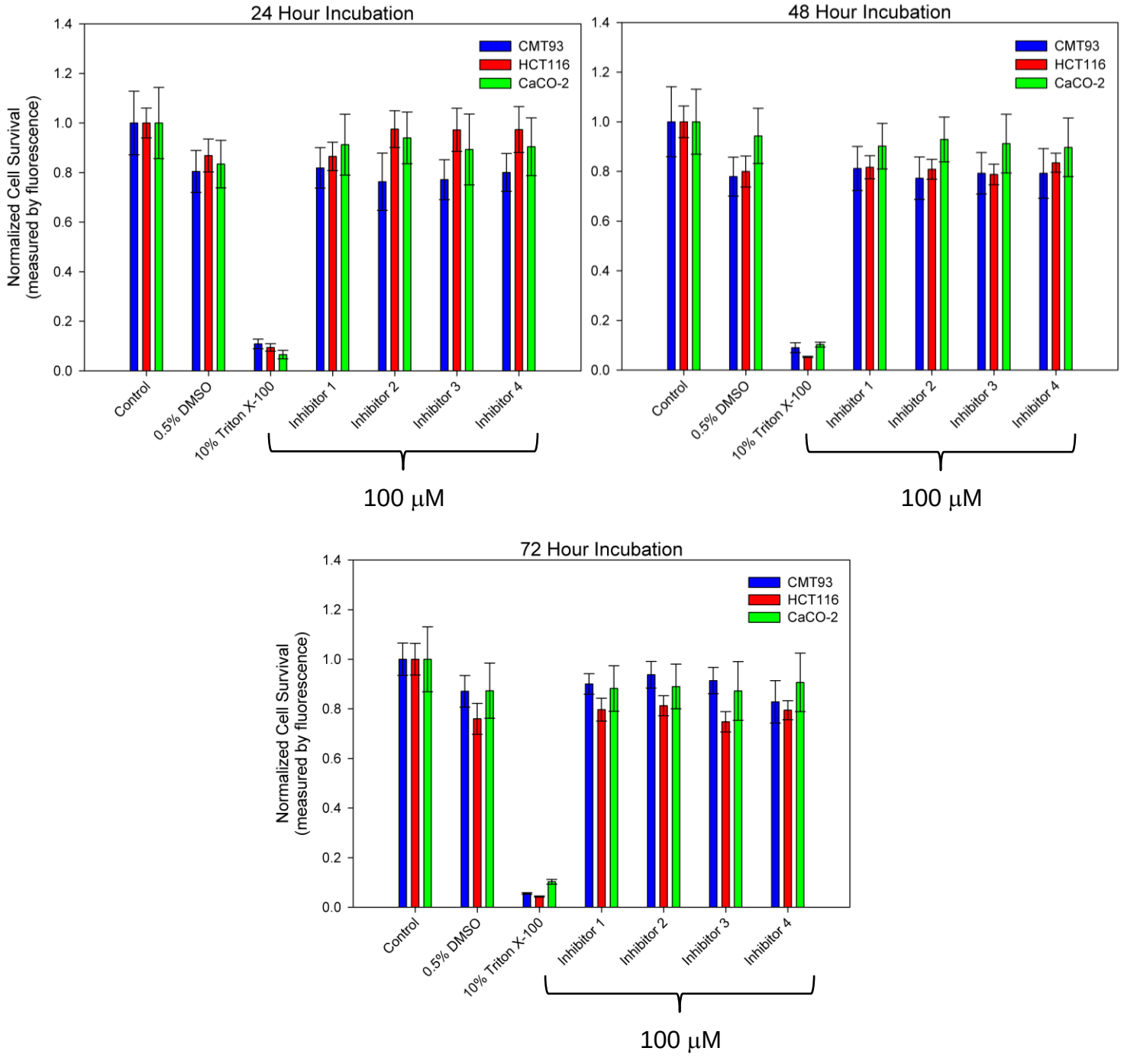

Fig. S18. Inhibitors 1-4 do not impact mammalian cell survival, unlike 10% Triton X-100. Any reduction in cell viability can be attributed to the presence of DMSO, as shown by the 0.5% DMSO control. CMT93 are murine colon cancer cells, CaCO-2 are human colon cancer cells, and HCT116 are human colon cancer cells. Error bars represent standard deviation, where N=4.

Fig. S19

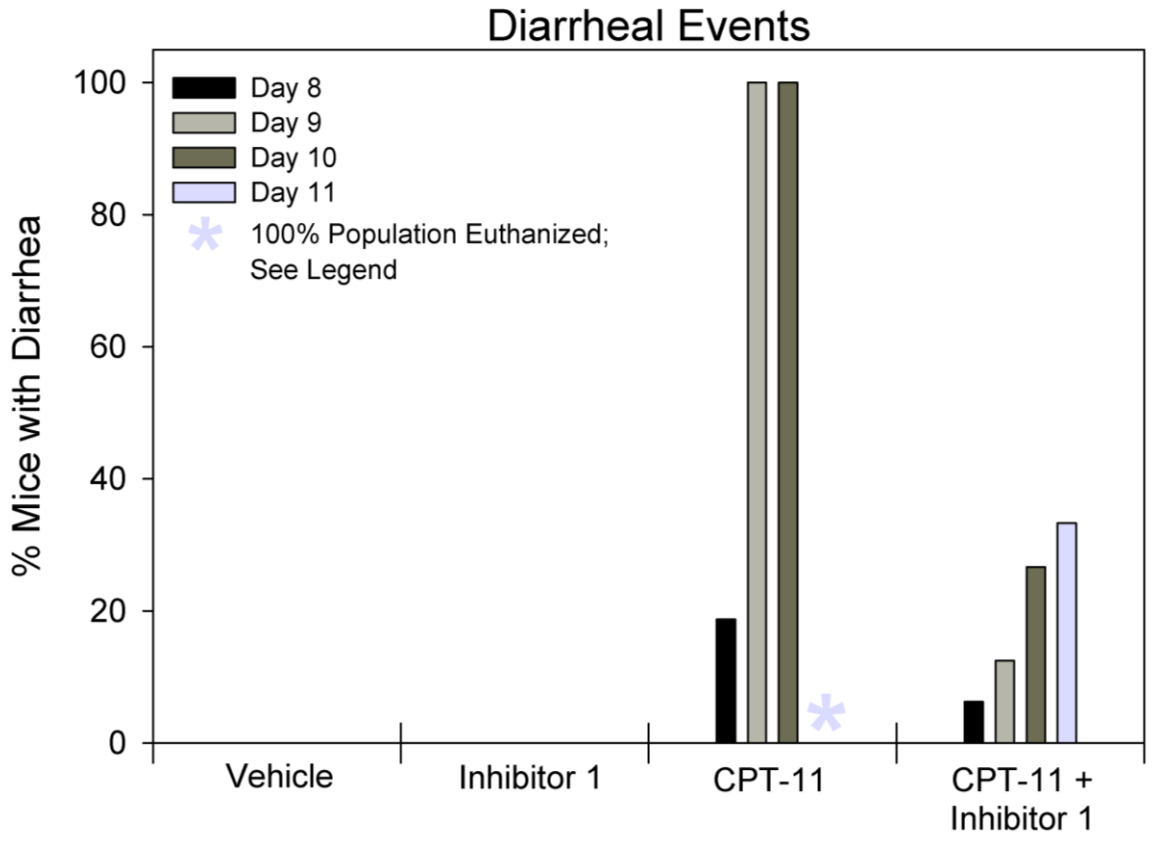

Fig. S19. CPT-11 induces diarrhea starting eight days after treatment initiation, while oral administration of Inhibitor 1 with CPT-11 reduces the incidents of diarrhea. Vehicle and Inhibitor 1 alone cause no diarrhea. By day 8-11 mice in the CPT-11 group began to suffer from severe lethargy and lack of movement, and as such, by day 11, all mice were euthanized according to AIC protocol 20070715.

Table S1

Data Collection

X-ray source	APS SER-CAT BM-22				
Space Group	C2				
Unit cell: a,b,c (Å); α,β,γ (°)	168.9, 77.3, 126.6; 90, 125.0, 90				
Data Set (PDB ID)	SeMet (3K4A)	Native (3K46)	GDL-bound (3K4D)	Inhibitor 2 (3LPF)	Inhibitor 3 (3LPG)
Wavelength (Å)	0.97926	1.0000	1.0000	1.0000	1.0000
Resolution (Å) (highest shell)	50.00-2.90 (3.00-2.90)	50.0-2.50 (2.59-2.50)	50.0-2.40 (2.49-2.40)	50.0-2.26 (2.32-2.26)	50.0-2.43 (2.47-2.43)
I/σ	22.9 (3.7)	21.9 (2.4)	35.2 (4.1)	36.2 (3.5)	26.6 (4.5)
Completeness (%)	99.2 (93.7)	96.5 (82.4)	98.6 (93.9)	96.9 (79.0)	98.2 (98.0)
Redundancy	7.4 (6.3)	5.2 (3.3)	7.0 (6.2)	6.8 (5.0)	3.9 (3.9)

Phasing and Refinement

	SeMet	Native	GDL-bound	Inhibitor 2	Inhibitor 3
Resolution (Å)	50-2.9	50-2.5	50-2.4	50-2.3	50-2.4
No. reflections	26483	43507	50982	56354	44902
Mean Figure of Merit	0.74				
R_{work}	0.242	0.214	0.204	0.208	0.204
R_{free}	0.282	0.267	0.237	0.249	0.246
Molecules per asymmetric unit (AU)	2	2	2	2	2
No. of amino acids per AU	1192	1194	1194	1206	1206
No. of waters per AU	214	358	355	398	358
Average *B*-factors	49.3	60.5	55.1	69.2	64.4
R.M.S. deviations					
Bond lengths (Å)	0.022	0.003	0.010	0.011	0.004
Bond angles (°)	1.920	0.815	1.520	1.594	1.023
Ramachandran (%)					
Preferred	96.7	97.0	98.4	95.3	97.3
Allowed	2.7	2.4	1.3	4.4	2.2
Outliers	0.6	0.6	0.3	0.3	0.5

Table S2

Actinobacillus succinogenes 130Z	Bifidobacterium gallicum DSM 20093
Akkermansia muciniphila ATCC BAA-835	Bifidobacterium longum DJO10A
Alistipes putredinis DSM 17216	Bifidobacterium longum infantis ATCC 15697
Bacteroides caccae ATCC 43185	Bifidobacterium longum infantis CCUG 52486
Bacteroides capillosus ATCC 29799	Bifidobacterium pseudocatenulatum DSM 20438
Bacteroides cellulosilyticus DSM 14838	Blautia hansenii VPI C7-24, DSM 20583
Bacteroides coprocola M16, DSM 17136	Blautia hydrogenotrophicus S5a33, DSM 10507
Bacteroides coprophilus DSM 18228	Catenibacterium mitsuokai DSM 15897
Bacteroides dorei DSM 17855	Clostridiales sp. 1_7_47_FAA
Bacteroides eggerthii DSM 20697	Clostridium asparagiforme DSM 15981
Bacteroides finegoldii DSM 17565	Clostridium bolteae ATCC BAA-613
Bacteroides fragilis 3_1_12	Clostridium hathewayi DSM 13479
Bacteroides fragilis YCH46	Clostridium hylemonae DSM 15053
Bacteroides intestinalis 341, DSM 17393	Clostridium leptum DSM 753
Bacteroides ovatus ATCC 8483	Clostridium nexile DSM 1787
Bacteroides plebeius DSM 17135	Clostridium ramosum DSM 1402
Bacteroides sp. 1_1_6	Clostridium scindens ATCC 35704
Bacteroides sp. 2_1_7	Clostridium sp. 7_2_43FAA
Bacteroides sp. 2_2_4	Clostridium sp. L2-50
Bacteroides sp. 3_2_5	Clostridium sp. SS2/1
Bacteroides sp. 4_3_47FAA	Clostridium spiroforme DSM 1552
Bacteroides sp. 9_1_42FAA	Collinsella stercoris DSM 13279
Bacteroides sp. D1	Coprococcus comes
Bacteroides sp. D2	Coprococcus eutactus ATCC 27759
Bacteroides sp. D4	Dorea formicigenerans ATCC 27755
Bacteroides stercoris ATCC 43183	Dorea longicatena DSM 13814
Bacteroides thetaiotaomicron VPI-5482	Escherichia coli 536
Bacteroides uniformis ATCC 8492	Escherichia coli APEC O1
Bacteroides vulgatus ATCC 8482	Escherichia coli ATCC 8739
Basfia succiniciproducens MBEL55E	Escherichia coli B7A
Bifidobacterium adolescentis ATCC 15703	Escherichia coli E110019
Bifidobacterium adolescentis L2-32	Escherichia coli E24377A
Bifidobacterium angulatum DSM 20098	Escherichia coli ED1a
Bifidobacterium animalis lactis AD011	Escherichia coli F11
Bifidobacterium breve DSM 20213	Escherichia coli HS
Bifidobacterium catenulatum DSM 16992	Escherichia coli K12 DH10B
Bifidobacterium dentium ATCC 27678	Escherichia coli O157:H7 EC508

T**able S2.** List of the 110 bacterial species that contain a β-glucuronidase or β-glucuronidase candidate, >50% of the bacterial loop, and contain a conserved residue in place of the L361 and F365 (see Fig. S13-S14). Data is derived from the June 29, 2010 search of the Human Microbiome Project Database (*S30*) search (Fig. S14). Continued on the following page.

Table S2 (cont.)

Escherichia coli O157:H7 EDL933
Escherichia coli O157:H7 Sakai
Escherichia coli SE11
Escherichia coli UTI89
Escherichia coli str. K-12 substr. MG1655
Escherichia sp. 1_1_43
Escherichia sp. 3_2_53FAA
Escherichia sp. 4_1_40B
Eubacterium eligens ATCC 27750
Eubacterium hallii DSM 3353
Eubacterium rectale ATCC 33656
Eubacterium ventriosum ATCC 27560
Faecalibacterium prausnitzii A2-165
Faecalibacterium prausnitzii M21/2
Fusobacterium mortiferum ATCC 9817
Holdemania filiformis VPI J1-31B-1, DSM 12042
Lactobacillus brevis ATCC 367
Lactobacillus brevis gravesensis ATCC 27305
Lactobacillus rhamnosus GG
Lactobacillus rhamnosus HN001
Lactobacillus rhamnosus LMS2-1
Lactobacillus rhamnosus Lc 705
Mitsuokella multacida DSM 20544
Mollicutes bacterium D7
Opitutaceae bacterium TAV2
Parabacteroides johnsonii DSM 18315
Parabacteroides merdae ATCC 43184
Prevotella copri CB7, DSM 18205
Roseburia intestinalis L1-82
Roseburia inulinivorans DSM 16841
Ruminococcus gnavus ATCC 29149
Ruminococcus lactaris ATCC 29176
Ruminococcus obeum ATCC 29174
Ruminococcus torques ATCC 27756
Sebaldella termitidis ATCC 33386
Shigella sp. D9

T**able S2 (cont.).** List of the 110 bacterial species that contain a β-glucuronidase or β-glucuronidase candidate, >50% of the bacterial loop, and contain a conserved residue in place of the L361 and F365 (see Fig. S13-S14). Data is derived from the June 29, 2010 search of the Human Microbiome Project Database (*S30*) search (Fig. S14).

Supplemental References

S1. Z. Otwinowski, W. Minor, Charles W. Carter, Jr., in *Methods Enzymol*. (Academic Press, 1997), vol. Volume 276, pp. 307-326.

S2. A. J. Howard, in *Crystallographic Computing 7: Proceedings from the Macromolecular Crystallographic Computing School* P.E. Bourne, K. D. Watenpaugh, Eds. (Oxford University Press, Oxford, 1996).

S3. P. D. Adams *et al.*, PHENIX: building new software for automated crystallographic structure determination *Acta Crystallogr D Biol Crystallogr* **58**, 1948 (Nov, 2002).

S4. P. Emsley, K. Cowtan, Coot: model-building tools for molecular graphics *Acta Crystallogr D Biol Crystallogr* **60**, 2126 (Dec, 2004).

S5. A. J. McCoy *et al.*, Phaser crystallographic software *J Appl Crystallogr* **40**, 658 (Aug 1, 2007).

S6. A. T. Brunger, Free R value: cross-validation in crystallography *Methods Enzymol* **277**, 366 (1997).

S7. A. W. Schuttelkopf, D. M. van Aalten, PRODRG: a tool for high-throughput crystallography of protein-ligand complexes *Acta Crystallogr D Biol Crystallogr* **60**, 1355 (Aug, 2004).

S8. A. W. Wong, S. He, J. H. Grubb, W. S. Sly, S. G. Withers, Identification of Glu-540 as the Catalytic Nucleophile of Human beta -Glucuronidase Using Electrospray Mass Spectrometry *J. Biol. Chem.* **273**, 34057 (December 18, 1998, 1998).

S9. V. Graef, E. Furuya, O. Nishikaze, Hydrolysis of steroid glucuronides with beta-glucuronidase preparations from bovine liver, Helix pomatia, and E. coli *Clin Chem* **23**, 532 (Mar, 1977).

S10. S. Reagan-Shaw, M. Nihal, N. Ahmad, Dose translation from animal to human studies revisited *Faseb J* **22**, 659 (Mar, 2008).

S11. G. Brandi *et al.*, Intestinal microflora and digestive toxicity of irinotecan in mice *Clin Cancer Res* **12**, 1299 (Feb 15, 2006).

S12. H. S. Cooper, S. N. Murthy, R. S. Shah, D. J. Sedergran, Clinicopathologic study of dextran sulfate sodium experimental murine colitis *Lab Invest* **69**, 238 (Aug, 1993).

S13. B. Siegmund *et al.*, Adenosine kinase inhibitor GP515 improves experimental colitis in mice *J Pharmacol Exp Ther* **296**, 99 (Jan, 2001).

S14. L. B. Saltz *et al.*, Irinotecan plus fluorouracil and leucovorin for metastatic colorectal cancer. Irinotecan Study Group *N Engl J Med* **343**, 905 (Sep 28, 2000).

S15. D. Cunningham *et al.*, Randomised trial of irinotecan plus supportive care versus supportive care alone after fluorouracil failure for patients with metastatic colorectal cancer *Lancet* **352**, 1413 (Oct 31, 1998).

S16. P. Rougier *et al.*, Randomised trial of irinotecan versus fluorouracil by continuous infusion after fluorouracil failure in patients with metastatic colorectal cancer *Lancet* **352**, 1407 (Oct 31, 1998).

S17. M. L. Rothenberg *et al.*, Phase II trial of irinotecan in patients with progressive or rapidly recurrent colorectal cancer *J Clin Oncol* **14**, 1128 (Apr, 1996).

S18. P. Rougier *et al.*, Phase II study of irinotecan in the treatment of advanced colorectal cancer in chemotherapy-naive patients and patients pretreated with fluorouracil-based chemotherapy *J Clin Oncol* **15**, 251 (Jan, 1997).

S19. Z. Guo *et al.*, Clinical pharmacokinetics (PK) of EZN-2208, a novel anticancer agent, in patients (pts) with advanced malignancies: A phase I, first-in-human, dose-escalation study *ASCO Meeting Abstracts* **26**, 2556 (May 20, 2008, 2008).

S20. A. J. Lu *et al.*, 3D-QSAR study of 20 (S)-camptothecin analogs *Acta Pharmacol Sin* **28**, 307 (Feb, 2007).

S21. R. H. J. Mathijssen *et al.*, Clinical Pharmacokinetics and Metabolism of Irinotecan (CPT-11) *Clin Cancer Res* **7**, 2182 (August 1, 2001, 2001).
S22. J. G. Slatter *et al.*, Pharmacokinetics, metabolism, and excretion of irinotecan (CPT-11) following I.V. infusion of [(14)C]CPT-11 in cancer patients *Drug Metab Dispos* **28**, 423 (Apr, 2000).
S23. G. G. Chabot *et al.*, Population pharmacokinetics and pharmacodynamics of irinotecan (CPT-11) and active metabolite SN-38 during phase I trials *Ann Oncol* **6**, 141 (Feb, 1995).
S24. G. G. Chabot, Clinical pharmacokinetics of irinotecan *Clin Pharmacokinet* **33**, 245 (Oct, 1997).
S25. R. H. Mathijssen *et al.*, Irinotecan pharmacokinetics-pharmacodynamics: the clinical relevance of prolonged exposure to SN-38 *Br J Cancer* **87**, 144 (Jul 15, 2002).
S26. L. Iyer *et al.*, Genetic predisposition to the metabolism of irinotecan (CPT-11). Role of uridine diphosphate glucuronosyltransferase isoform 1A1 in the glucuronidation of its active metabolite (SN-38) in human liver microsomes *J Clin Invest* **101**, 847 (Feb 15, 1998).
S27. G. Szasz, Comparison between p-nitrophenyl glucuronide and phenolphthalein glucuronide as substrates in the assay of beta-glucuronidase *Clin Chem* **13**, 752 (Sep, 1967).
S28. L. Holm, S. Kaariainen, P. Rosenstrom, A. Schenkel, Searching protein structure databases with DaliLite v.3 *Bioinformatics* **24**, 2780 (Dec 1, 2008).
S29. J. D. Thompson, T. J. Gibson, D. G. Higgins, Multiple sequence alignment using ClustalW and ClustalX *Curr Protoc Bioinformatics* **Chapter 2**, Unit 2 3 (Aug, 2002).
S30. P. J. Turnbaugh *et al.*, The human microbiome project *Nature* **449**, 804 (Oct 18, 2007).